Chapter 5
Role of thiol-mixed-co-surfactant in Reduction of Energy Barrier

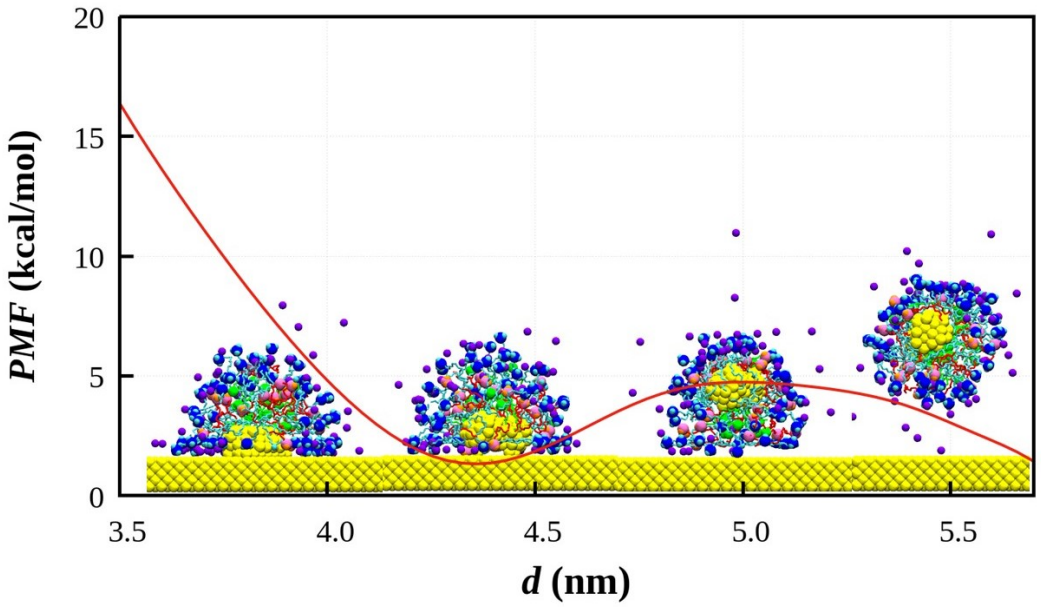

5.1 Introduction

Over the past two decades, amphiphilic molecules have garnered significant interest from both fundamental research and industrial applications. This is largely attributed to their ability to exhibit diverse aggregation behavior when mixed with water and other organic species. Key properties such as micelle sizes, shapes, shape transitions, critical micellar concentrations (CMC), and the effects of temperature on micelle sizes and shapes have been studied in detail. Theoretical studies have provided valuable insights into these phenomena.[60] Their amphiphilic nature promotes the formation of self-assembled mesoscopic structures, such as spherical micelles, at moderate surfactant concentrations.[75] At higher concentrations, or with the inclusion of electrolytes[196] or organic additives (co-surfactants), such as oleylamine[174, 175], thiols[173], sodium dodecylsulphate[197]

etc., cylindrical micelles can form and achieve stabilization.[198] As the surfactant concentration continues to rise, more complex structures emerge, including vesicles[136] and bilayers[199], expanding the versatility and functionality of these systems.

The role of mixed surfactants in micelle-mediated nanocrystal formation has gained increasing attention, particularly for systems involving gold nanocrystals due to their size-dependent optical[41, 159], electrical[42], and catalytic[127] properties. These unique characteristics underpin their widespread use in plasmon-enhanced spectroscopies[200, 201], catalysis[4, 126, 157], sensing[120, 121], photonics[202], optics[203], biomedicine[125, 129, 130, 204, 205], bioimaging[128, 204], biosensing [206, 207] and nanoelectronics.[115, 118] However, achieving precise control over their morphology and monodispersity requires a fundamental understanding of the energetics and kinetics of the nucleation process.

Conventional nucleation theories such as LaMer-Brust burst nucleation[44], Ostwald ripening[45], the Finke-Watzky slow continuous growth model[46], and mechanisms like oriented attachment or coalescence[47, 166] have been applied to explain nanocrystal formation in solution.

As a first step, we aim to understand how such surfactant systems influence nucleation processes at the molecular scale, particularly within aqueous environments, where micellar structures, interfacial dynamics, and co-surfactant interactions play a critical role in directing nanocrystal formation. Molecular dynamics (MD) simulations were employed to quantify micelle sizes formed by CTAB molecules in aqueous solutions. CTAB micelles have been extensively studied as templates for the anisotropic growth of nanoparticles, such as gold nanorods. Murphy et al. demonstrated that CTAB micelles promote the anisotropic growth of gold nanorods by stabilizing specific crystal facets, especially the 110 surface, through strong surfactant adsorption [143]. The addition of co-surfactants like oleylamine and thiols enhances this effect by modulating micelle shape and interaction with precursors. Jana proposed that elongated micelles formed by CTAB play a pivotal role in directing anisotropic growth, which is further influenced by temperature

and surfactant concentration [208]. Thiol molecules, on the other hand, strongly interact with metal surfaces and are known for their functionalization and stabilization properties. While their direct role in forming cylindrical micelles is limited, they significantly influence micelle-mediated nanoparticle synthesis by altering surface properties and stability [31].

The addition of oleylamine and thiols to CTAB solutions not only changes the micelle morphology but also impacts their interaction with ionic precursors and substrates. Wang and Larson demonstrated that the addition of salts or co-surfactants induces sphere-to-cylinder transitions in micelles by modulating electrostatic interactions [74]. Suárez-López et al., using dissipative particle dynamics (DPD) simulations, showed that surfactants play a critical role in controlling the nucleation and growth of nanoparticles by altering the micelle morphology and interfacial properties [182].

Thiol molecules, due to their strong affinity for metal surfaces, are frequently used in nanoparticle synthesis and stabilization. Meena et al. observed that the interstitial space between CTAB micelles facilitates the direct diffusion of ionic precursors like $AuCl_2^-$, resulting in preferential crystal growth along the (111) facet [145]. Thiol-functionalized systems are also employed to enhance micelle stability and guide nanoparticle assembly through molecular recognition and mucoadhesion [209].

In our previous chapter 4, we have seen the role of co-surfactant OLA on the nucleation and its growth on a surface, along with primary surfactant CTAB and investigated the energy barrier by calculating the potential of mean force.[210]

In this chapter, we extend our investigation by introducing hexadecanethiol (HDT) as an additional cosurfactant alongside oleylamine (OLA) and cetyltrimethylammonium bromide (CTAB) to further optimize the nucleation and growth of gold nanocrystals. While the combination of CTAB and OLA proved effective in transforming micelle structures from spherical to cylindrical or elongated forms, a significant energy barrier persisted during the nucleation process due to the strong layering of water molecules on the gold surface.

5.2 Model & Methodology

To make this system, we randomly distributed 60 CTAB molecules, 20 OLA molecules, and 20 hexadecanethiol (HT) molecules, represented as SH-$(CH_2)_{15}CH_3$ in a simulation box of 9 nm $\times$ 5.8 nm $\times$ 12 nm containing 16000 water molecules. HT was treated as a 16-carbon alkyl chain with a thiol headgroup, using united atoms for CH_2 and CH_3 groups. GROMOS96 53a6 forcefield[93] was used to model the bonded and non-bonded interactions for CTAB, OLA and HT molecules. An extended Simple Point Charge (SPC/E) water model was used to model the solvent. The charge on the CTA cation was such that the three methyl groups in the headgroup carried a partial positive charge of 0.1701e, the methyl group adjacent to nitrogen carried a partial positive charge of 0.2167e, and the methyl groups in the tail group were set to be neutral. The central nitrogen atom was set to be 0.273e, and the bromide ions carry a charge of -1. The nitrogen atom in the amine group of co-surfactant OLA was set to be – 0.892e, both the hydrogen atoms attached to the nitrogen in the amine group were set to be 0.356e each, the methyl group in the tail group of OLA was set to be 0.180e and rest groups in the OLA were set to be neutral. The charge on the sulfur atom in the thiol group of co-surfactant HT was set to be -0.171e, and the charge on the carbon atom in the methyl group attached to the thiol was set to be 0.171e. The rest groups in the HDT were set to be neutral. All the molecules were kept fully flexible.

The nonbonded interactions between like and alike particles were modelled as per Lennard-Jones 12-6. The bond stretching and bending were described using harmonic potentials. For nonbonded interactions, a cutoff distance of 12 Åwas used. All MD simulations were performed using LAMMPS software.[211] VMD[150] was used to visualize the simulation trajectories. The simulation box was considered periodic in all three directions. The initial configuration of a cylindrical micelle was subjected to energy minimization for 5,000 steps using the steepest descent method. The temperature and pressure were maintained by the Nosé-Hoover thermostat (relaxation time is 0.5 ps) [212] and the Parrinello-Rahman barostat (relaxation time is 1.0 ps)[105], respectively. The solution was equili-

brated in an NPT ensemble for 5 ns. Molecular dynamics production runs were performed in an NVT ensemble for 60 ns with a timestep of 2 fs to integrate the equation of motion using the Velocity Verlet algorithm.[89] The trajectory was stored every 1 ps. Long-range electrostatic interactions were calculated using the particle-particle particle-mesh (PPPM) method[98] with a real space cut-off of 1 nm, a grid spacing of 0.8 nm, and an interpolation order of 10^{-4}. Bonds and angles were constrained using the SHAKE algorithm.[100]

Figure 5.1(a), (b) and (c) displayed the molecular models of CTAB, OLA and HT molecules, respectively, showing the building units of the molecules. The hydrophilic headgroups are encircled to show an explicit model, while the hydrophobic tails are represented in cyan for CTAB, red for OLA, and sky blue for HT, considering the united atom model. The simulation box was considered periodic in all three directions. An energy minimization procedure of 5000 steps using the steepest descent method ensured system stability. After 60 ns production run, the CTAB, OLA, and HT molecules self-assembled into a cylindrical micelle as shown in Figure 5.1 (d), with alkyl tails forming the hydrophobic core and sulfur atoms of the thiol groups orientated outward, demonstrating the structural organization of the micelle in aqueous solution. All the interaction parameters used in this study are listed in Table 5.1.[213]. We use the Lorentz-Berthelot combination rules for the cross-interaction parameters.[214]

Further, we randomly distributed 100 gold atoms in the solution, allowing the formation of nucleates of varying sizes and shapes. The energy landscape for the fusion of nucleates with the gold surface was calculated using the umbrella sampling technique[155] followed by the Weighted Histogram Analysis Method (WHAM) [154]. In the umbrella sampling, a series of 70 linearly spaced windows along the reaction coordinate, defined by the distance between the centre of mass of the nucleate and the apex of the gold surface, were subjected to an external biasing potential to facilitate comprehensive sampling within these windows. A harmonic potential, $u_i = \frac{1}{2}k(r - r_i)^2$ used as the external biasing potential at window i, where r_i represents the reference location and k denotes the harmonic force constant. We utilised the Weighted Histogram Analysis Method (WHAM) to remove the biasing potential and reconstruct the potential of mean force (PMF).[154] The reaction co-

Table 5.1: Force Field Parameters for Hexadecanethiol Molecules.

Nonbonded Interactions				
Atom	σ_{ij} **(Å)**	ϵ_{ij} **(kcal/mol)**	q **(e)**	
CH_3	3.75	0.194	0.0	
CH_2	3.75	0.091	0.171	
SH	3.62	0.461	-0.171	
Bond-stretching				
Bond	r_0 **(Å)**	k_b **[kcal/mol.Å^2]**		
CH_2-CH_3	1.52	200		
CH_2-CH_2	1.54	200		
S=H	1.82	200		
Bending				
Angle	θ_0 **(Å)**	k_θ **[kcal/mol.Å^2]**		
CH_2-CH_2-CH_3	114	124.216		
H-S-CH_2	96	67.18638		
Torsion (kcal/mol)				
Dihedral	k_1	k_2	k_3	k_4
H-S-CH_2-CH_2	0.1032	-0.1033	0.0366	0.6084
CH_2-CH_2-CH_2-CH_3	0.0	0.7056	-0.1355	1.5727

ordinate defined as the distance between the center of mass of gold nucleate and the upper surface of the gold (111) surface was the reaction coordinate. A 1.0 ns production runs were conducted in an NVT ensemble for each window at 303.15 K, employing restraints with a harmonic force constant of 100 kcal/mol.Å^2. In WHAM, the calculation of PMF involved setting the number of bins to 100, accompanied by a tolerance for iterations of 10^{-5}. We monitored the size and shape of the micelle by calculating the components of the radius of gyration (R_g) tensor, $R_{g_{xx}}$, $R_{g_{yy}}$, $R_{g_{zz}}$, respectively. The radius of gyration R_g of the micelle was calculated using the equation: $R_g = \sqrt{(\sum_{i=1}^{N}(R_i - R_{COM})^2)/N}$ where, N is the total number of atoms in the micelle, R_{COM} is the center of mass (COM) of that micelle, and R_i is the position of the i^{th} atom in the micelle. We calculated the order parameter to understand the orientation of the molecules within the micelle on the gold surface. The order parameter of the micelle molecules is a measure of the degree of ordering and alignment of CTAB molecules within a micelle structure. The order parameter expressed as $S_{zz} = (3cos^2\theta_i - 1)/2$ where, θ_i is the angle between the end-to-end vector of the i^{th} molecule and the surface normal vector.

Figure 5.1 (d) represents a snapshot of a cylindrical micelle formed by a mixture of CTAB,

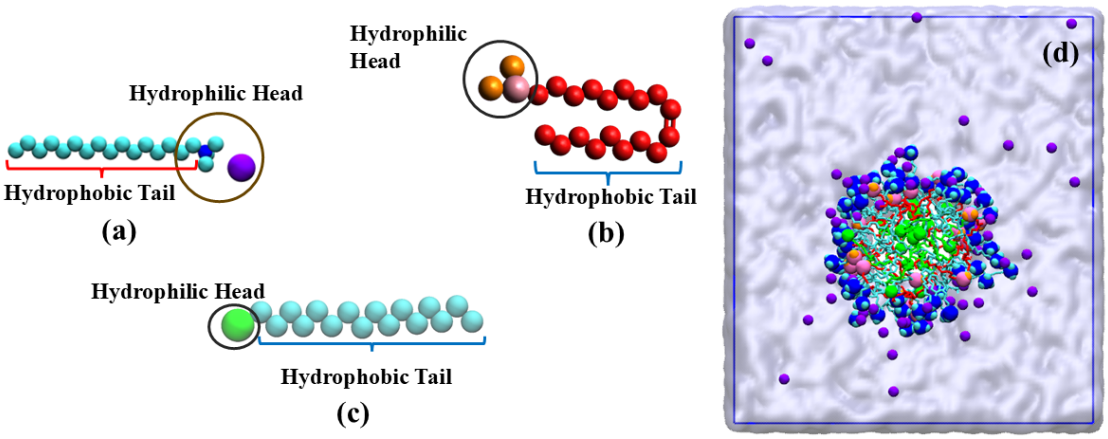

Figure 5.1: Molecular representation of the molecules – (a) CTAB, (b) Oleyamine and (c) Hexadecanethiol – indicating their hydrophilic head and hydrophobic tail groups. For CTAB, the methyl groups, nitrogen atoms and bromide ions are represented as cyan, blue and purple spheres, respectively, whereas for oleylamine, the methyl groups, nitrogen atoms and hydrogen atoms are represented as red, pink and orange spheres, and for hexadecanethiol, the methyl groups and thiol group are represented sky blue and green spheres respectively; (d) Snapshot of the cylindrical micelle formed by CTAB, OLA, and thiol molecules along y-axis after 10 ns production run. For the CTAB molecule, the nitrogen atoms and bromide ions are represented as blue and purple spheres, respectively, and all the methyl groups are represented as cyan spheres. For the oleylamine molecule, the nitrogen atoms and hydrogen atoms are represented as pink and orange spheres, respectively, and all the methyl groups are represented as red spheres. For the Hexadecanethiol molecule, the thiol group is represented as a green-coloured sphere, and all the methyl groups are represented as green color lines. Water has shown an ice-blue colour in continuous media. The blue rectangle represents the periodic box.

OLA, and HT molecules after a 10 ns run. We have initially randomly distributed the CTAB, OLA, and HT molecules in water. Through molecular dynamics simulations, these molecules self-assembled into a micellar structure driven by hydrophobic interactions among their alkyl tails. The hydrophobic tails aggregated to form the nonpolar inner core of the micelle, while the polar head groups oriented themselves toward the surrounding water molecules and ions, stabilizing the micelle in the aqueous environment.

5.3 Results and Discussion

We begin by exploring the role of co-surfactants, oleylamine (OLA) and thiol, in conjunction with CTAB, in driving the formation of cylindrical micelles within the solution. To gain a detailed understanding of the structural organization and stability of the CTAB-OLA

micelles, we will analyze several key parameters. First, the density profiles of individual components, such as the alkyl chains, head groups, co-surfactants, and solvent molecules, will be examined. Second, the radial distribution functions (RDF) will be analyzed to quantify the interactions and spatial relationships between specific atomic or molecular groups, such as the oxygen of water molecules with the nitrogen in the CTAB head group, the nitrogen in OLA, and the sulfur in the thiol group. Furthermore, the radius of gyration R_g will be calculated as a measure of the overall size and compactness of the micelle. Variations in R_g with temperature were calculated. The study then transitions to quantifying the nucleation process within the micellar environment, focusing on the formation and subsequent engulfment of gold nucleates by the cylindrical micelle. Finally, the free energy landscape for the engulfment process will be estimated, with particular emphasis on the adherence of the gold nucleate to a gold (111) surface. This involves calculating the potential of mean force (U_{PMF}) as a function of distance, providing insights into the stability of the gold nucleate at different positions relative to the surface.

Figure 5.2 depicted the structural and thermodynamic properties of a CTAB-based cylindrical micelle in the presence of co-surfactants (oleylamine and thiol), focusing on density distribution, radial distribution functions (RDFs), and radius of gyration. Figure 5.2(a) shows the mass density profiles of various micelle components as a function of radial distance (r) from the micelle's centre of mass at 303 K. The hydrophobic core is dominated by CTAB alkyl chains, with a peak near ~ 0.5 nm. The hydrophilic core consists of the ammonium head groups of CTAB, the amine groups of OLA, and the thiol group of HT located near ~ 1.5 nm. Bromide ions are distributed in the intermediate region, stabilizing the micelle-water interface, while water molecules surround the micelle's outer layer. These profiles confirm the formation of a well-defined cylindrical micelle with distinct hydrophobic and hydrophilic regions. Figures 5.2 (b), (c), and (d) present the RDF of water oxygen atoms with the nitrogen in CTAB's ammonium head group, the nitrogen in OLA's amine group, and the sulfur in the thiol group, respectively, at different temperatures. In Figure 5.2(b), a prominent peak at ~ 0.4 nm indicates a strong and temperature-independent hydration shell around CTAB's head group. Figure 5.2(c) revealed a similar

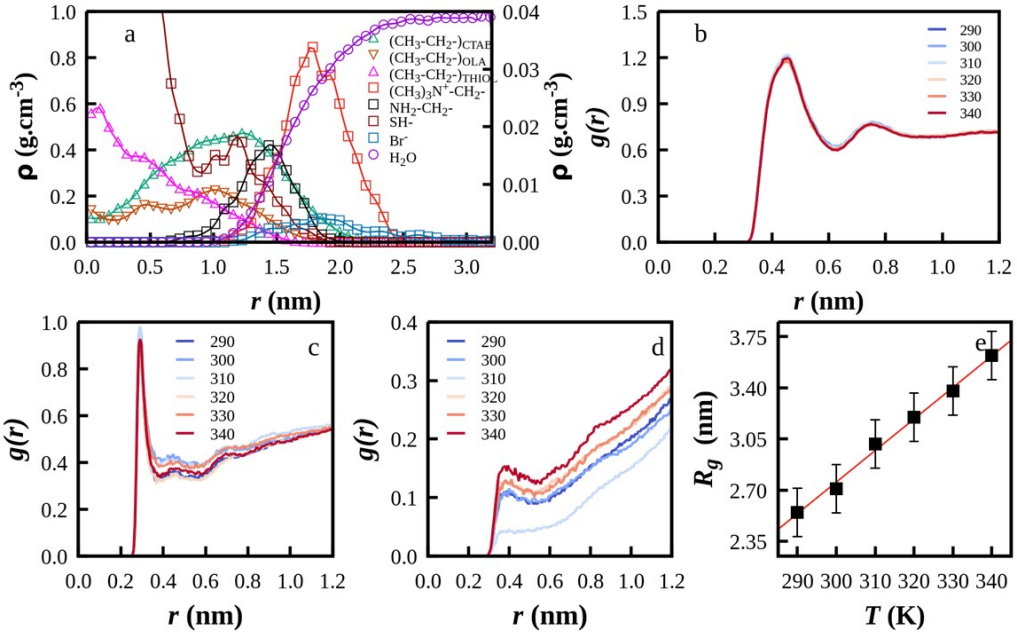

Figure 5.2: (a) Mass density profiles of different segments; alkyl chain of CTAB, OLA and thiol, ammonium group, amine group, thiol group, bromide ions, and water as a function of distance from the centre of mass of a CTAB micelle at 303 K. The density profile of the ammonium group of CTAB, the amine group of co-surfactant OLA and the thiol group of co-surfactant HT are plotted on the right-side y-axis and rest on the left-side y-axis. (b) Radial distribution functions between the Oxygen of water and N of the head group of CTAB surfactant at different temperatures, (c) Radial distribution functions between the Oxygen of water and N of the head group of co-surfactant OLA at different temperatures, (d) Radial distribution functions between the Oxygen of water and Sulfur of the thiol group of co-surfactant Thiol at different temperatures, (e) Radius of gyration of the micelle is plotted at different temperatures.

sharp peak near ~ 0.4 nm, showing strong interactions between OLA's hydrophilic region and water. In Figure 5.2(d), the RDF between water oxygen and the thiol sulfur exhibits a weaker peak at ~ 0.4 nm, indicating reduced hydration due to the lower polarity of the thiol group. The increase in peak intensity with temperature suggests enhanced diffusion and interaction of water near the thiol group at higher temperatures. Figure 5.2(e) displays the radius of gyration of the cylindrical micelle as a function of temperature. The linear increase in (R_g) with temperature indicates that the micelle expands as the temperature increases, likely due to increased thermal motion and reduced hydrophobic interactions.

Figure 5.3 (a) depicts the process of gold nucleation within a CTAB-OLA-thiol micelle system, indicating the time-dependent evolution of nucleates and structural changes in the micelle. Figure 5.3(b) shows the number of nucleates as a function of simulation time (t)

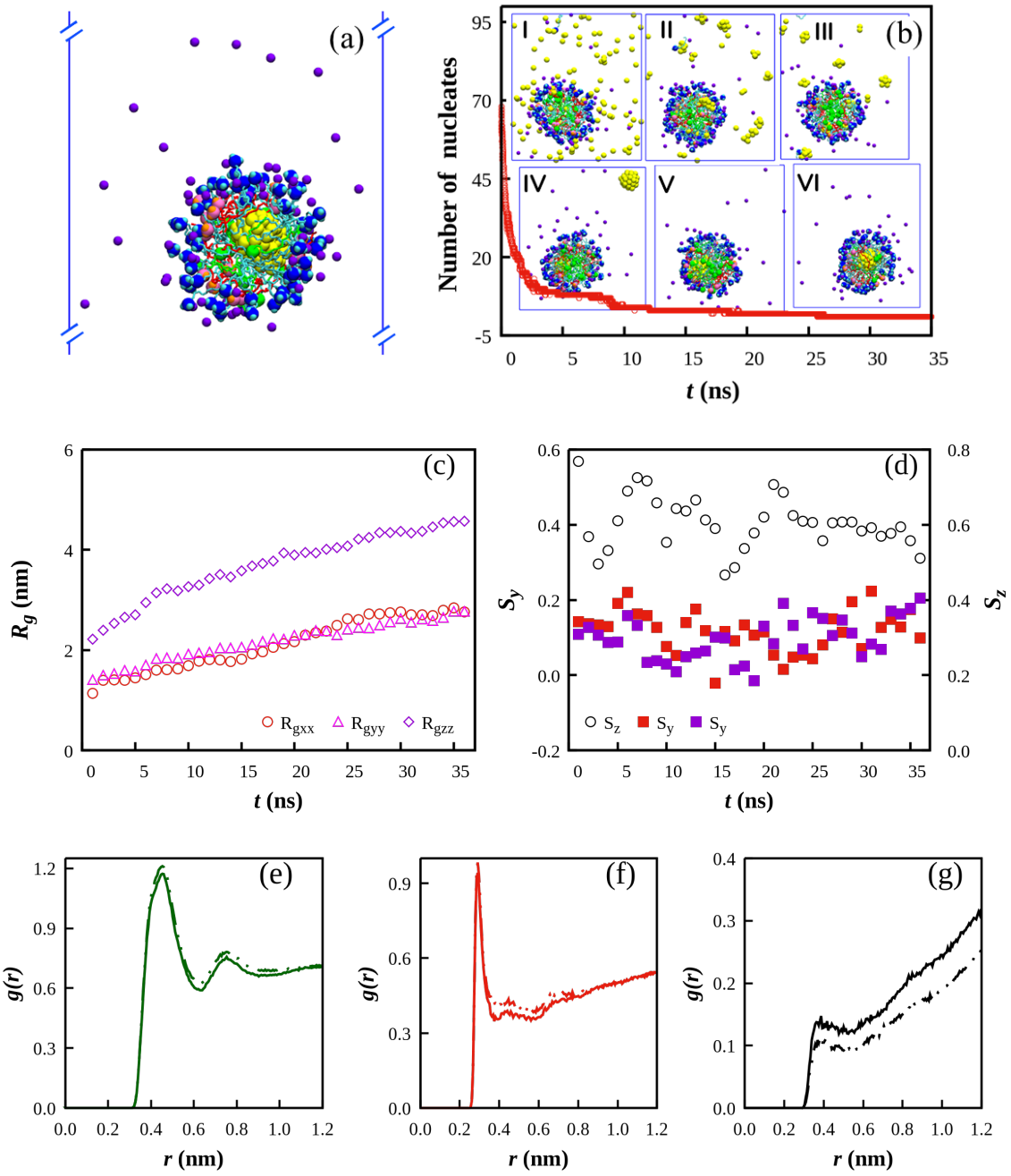

Figure 5.3: (a) Formation of Gold nucleates inside the micelle in an aqueous solution. (b) Formation of the number of nucleates as a function of time, Insets (I-VI) contain the snapshots of nucleate formation at 0, 1, 2, 15, 25, and 35 ns. (c) The radius of gyration of the micelle with time. (d) The change in order parameter of OLA molecules and Thiol molecules in the y-direction (left axis) and CTAB molecules in the z-direction (right axis). Color codes for molecular presentation are the same as in Figure 5.1; water is omitted for clarity. (e,f,g) Comparison of RDF between the head group of surfactant molecules (green: CTAB, red: OLA and black: THIOL) and water molecules after engulfing nucleates (solid lines) and that of a pure micelle (dashed line), respectively.

along with representative snapshots of the nucleation process at six distinct times (0, 1, 2, 15, 25, and 35 ns). The initial random distribution of gold atoms at 0 ns (Inset I) leads to the formation of nucleates of distinct shapes and sizes. The number of nucleates decreases rapidly in the initial phase of the simulation (1 ns), Inset II, indicating a coalescence of smaller nuclei into larger aggregates, driven by the attractive forces and micelle-induced confinement. Over time, the system stabilizes with a smaller number of larger nucleates, as shown in Insets (III-VI). Figure 5.3(c) tracks the radius of gyration (R_g), representing the overall size of the micelle. The components R_g of along different axes (R_{gxx}, R_{gyy}, and R_{gzz}) show a clear anisotropy, with R_{gzz} increasing more significantly than R_{gxx} and R_{gyy}. This indicates the elongation of the micelle along its principal axis, driven by the growth and accommodation of nucleates. Figure 5.3(d) shows the changes in the micelle's structural order and size during the simulation. The left axis shows the time-dependent evolution of the order parameter (S_{zz}), which quantifies the alignment of molecules along the cylindrical micelle's principal axis. The increase in S_{zz} over time reflects enhanced molecular alignment and structural stabilization of the micelle as nucleation progresses. Initially, S_{zz} is low due to the random orientation of molecules, but as nucleates form and grow, the micelle adapts its shape to accommodate them, increasing the alignment of the surfactant and co-surfactant molecules. In Figure 5.3(e) and (f), the comparison of RDF between the surfactant head groups and water molecules suggests that the incorporation of nucleates does not significantly displace water. This is evident from the minimal change in RDF peak values between the pure micelle (dashed lines) and the nucleate-engulfed micelle (solid lines). Instead, the presence of nucleates appears to modify the micelle structure in a way that enhances hydration. This is because the nucleate incorporation leads to micelle expansion or changes in its curvature, thereby increasing the accessibility of surfactant head groups to water molecules. If micelle deformation occurs, it may expose more head groups to the solvent, resulting in a higher local water density near the interface. Notably, the higher RDF peak in Figure 5.3(g) suggests stronger structuring of water around the surfactant head groups, indicating that the altered micelle conformation promotes a more ordered hydration shell.

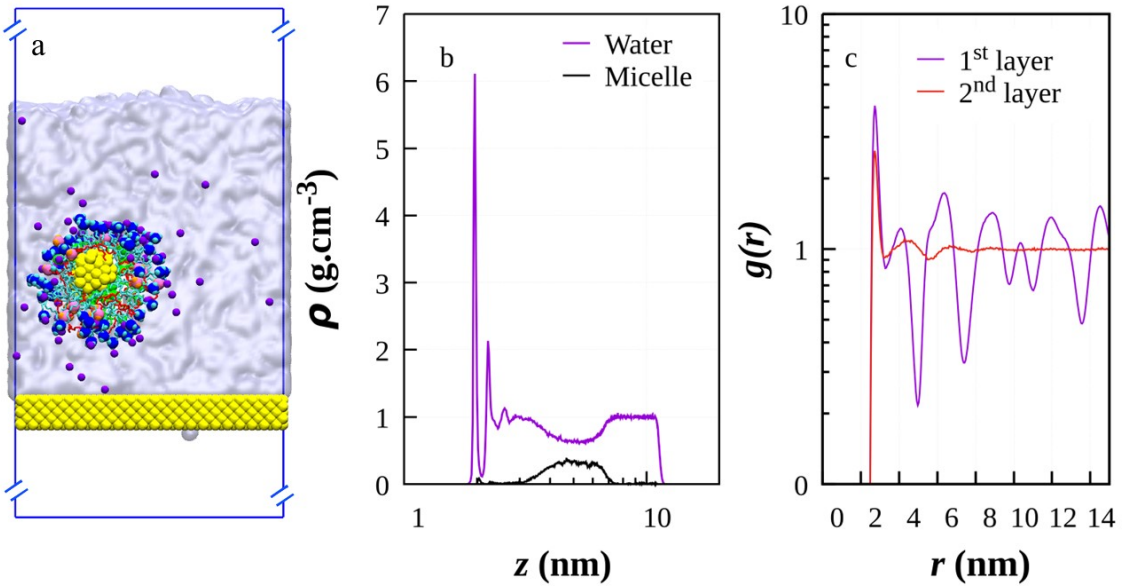

Figure 5.4: (a) Snapshot of the system containing a cylindrical micelle of co-surfactant OLA and thiol with CTAB molecules away from the gold surface in an aqueous media. The Au(111) surface, at the bottom, is represented in yellow spheres. Water has shown an ice-blue color continuous media. The blue rectangle represents the periodic box (not to scale in the z-direction). (c) Mass density of water and micelle as a function of distance from Au (111) gold surface.(c) In-plane pair correlations (radial distribution function) between water molecules in the layer adjacent to the Au(111) gold surface.

The cylindrical micelle engulfed gold nucleates were initially far from the gold surface, as shown in Figure 5.4a, and remained stable in the aqueous medium. Even after a ~ 45 ns simulation, the micelle did not migrate to the surface, indicating the presence of a significant energy barrier. To quantify this barrier, we performed PMF calculations using Umbrella sampling. However, before applying any external force on the engulfed micelle, it was essential to identify the underlying cause of the energy barrier preventing the micelle's approach to the surface. This barrier comes primarily from the strong layering of water molecules on the Au(111) surface. To investigate this behavior, we computed the density profile and the radial distribution function, as presented in Figures 5.4b and 5.4c.

Figure 5.4(b) depicts the density profiles of water and the micelle as a function of distance from the gold surface. The sharp peak in the water density profile, represented by the blue line near the surface (at ~ 2.0 nm), indicated the presence of a high-density water layer strongly adsorbed onto the gold surface. This corresponds to the 1^{st} layer of water molecules observed in Figure 5.4(c), where the high peak signifies a highly ordered

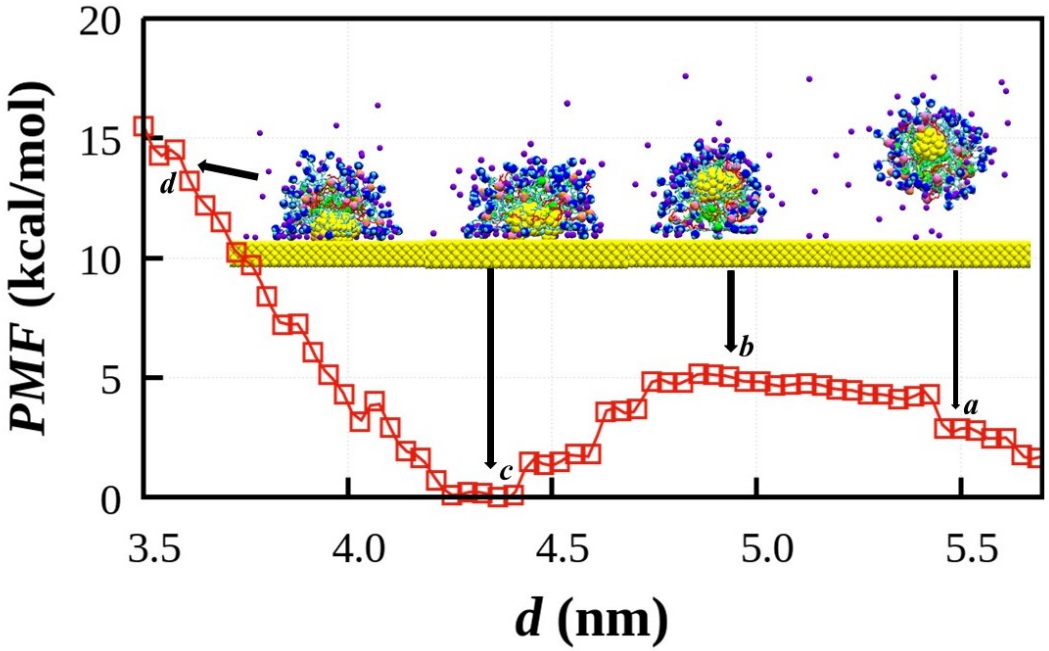

Figure 5.5: Potential of mean force between the centre of mass of gold nucleate and the top of the gold (111) surface. Snapshots inside the plot show the relative positions of nucleate and micelle on the surface. The black arrows indicate the nucleate's position from the apex of the gold surface. The color codes for molecular presentation are the same as in Figure 5.1, and water is omitted for visual clarity.

arrangement of water molecules due to strong adsorption and surface interactions. This dense, ordered water layer creates a significant energy barrier that the micelle must overcome to reach the gold surface, as highlighted in Figure 5.4(b). A second strong peak in the water density profile observed at ~ 3.87 nm in Figure 5.4(b), aligns with the 2^{nd} layer of water molecules shown in Figure 5.4(c). This layer is less ordered but still structured, forming due to interactions between water and the micelle molecules. The micelle density profile in Figure 5.4(b), represented by the black line, reflects these interactions, showing a distinct peak at ~ 4.74 nm, which corresponds to the micelle's equilibrium position relative to the gold surface. The broadening of the water density near the micelle suggests the formation of a diffuse hydration layer surrounding the micelle, which stabilizes its structure and maintains its integrity in the aqueous medium. Beyond this region, the water density stabilizes, reaching a constant value characteristic of the bulk water phase. This interplay between the hydration layers and the micelle highlights the structural and dynamic factors influencing micelle behavior near the gold surface.

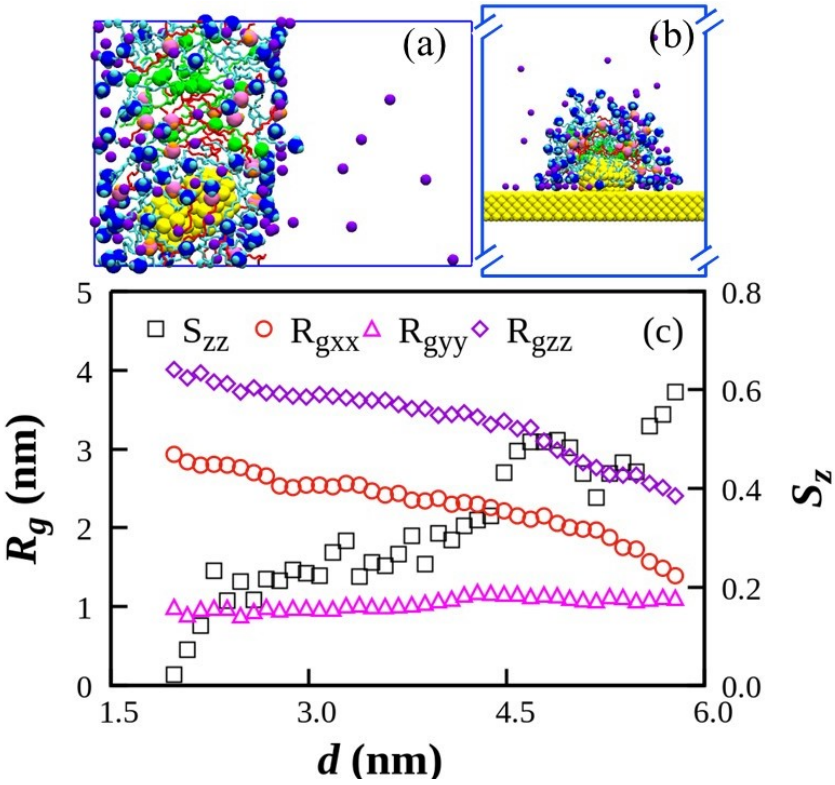

Figure 5.6: The top view and side view of a micelle containing nucleate are shown in (a) and (b), respectively. The color codes for molecular presentation are the same as in Figure 5.1; the gold surface and water molecules are omitted for clarity. (c)The radius of gyration (left axis) and change in order parameter (right axis) of the micelle with distance between the centre of mass of the gold nucleus and the top of the gold (111) surface.

To gain deeper insight into the energy landscape of a gold nucleate engulfed in a cylindrical micelle and its movement toward a gold (111) surface, we calculated the Potential of Mean Force (PMF) between the centre of mass of the gold nucleate and the top of the gold (111) surface. At larger distances $\sim$ 5.6 nm, the PMF is low (2.45 kcal/mol) at point "a," a low energy state, indicating that the micelle is more stable in bulk solution. Due to strong repulsive forces or an energy barrier of 2.83 ± 0.12 that prevents the engulfed micelle from spontaneously approaching the surface as represented by point "b" in Figure 5.5. Further, the PMF started decreasing as the micelle moved closer to the surface, suggesting a gradual reduction in the energy barrier. The PMF curve reached its minimum near point "c" at $\sim$ 4.0 nm, indicating the most energetically favourable position for the engulfed micelle. As the micelle moves even closer, there is an increase in PMF, indicating a secondary energy barrier as shown at point "d" in the Figure 5.5. This is due to van der Waals repulsion between the nucleate and the surface.

Figures 5.6a and 5.6b present the top and side views of a micelle containing a gold nucleate, offering a detailed visualization of structural changes during its interaction with the gold surface, especially near the gold surface. The top view (Figure 5.6a) revealed significant deformation of the micelle to accommodate the nucleate, highlighting its adaptability. The side view (Figure 5.6b) demonstrates that the micelle elongates or deforms as it interacts with the nucleate, likely due to the influence of the gold surface. This deformation is crucial for accommodating the growing nucleate while maintaining the micelle's overall stability. To quantify the micelle deformation during this process, we calculated the radius of gyration (R_g) and order parameter (OP) as a function of the distance between the centre of mass (COM) of the gold nucleate and the surface. R_{gzz} is initially higher, indicating more extended micelle structures in the lateral z-direction. This decreases as the micelle approaches the surface, suggesting structural compression. R_{gxx} is relatively lower throughout, reflecting a more compact structure in the x-direction. R_{gyy} is constant throughout the distance. The order parameter (S_z) increases as the micelle approaches the gold surface, indicating an increasing degree of alignment or ordering of micelle components along the z-axis. This ordering is likely driven by interactions between the gold surface and the polar or charged groups within the micelle. At larger distances, ~ 5.5 nm, the micelle retains a cylindrical shape, as evidenced by lower R_{gxx} and R_{gzz}. The order parameter (S_z) remains high, reflecting more alignment structure. At shorter distances, where the nucleate is in close proximity to the gold surface, S_z is lower, indicating disruption in the alignment of the surfactant molecules. This may be caused by the interaction between the nucleate and the surface, which perturbs the micelle's structure.

5.4 Summary

The study delved into the influence of hexadecanethiol (HDT) as a co-surfactant in conjunction with oleylamine (OLA) and cetyltrimethylammonium bromide (CTAB) on micelle dynamics and gold nucleation processes. The introduction of HT was shown to significantly modify the structural organization of the micelles, transitioning their morphology from spherical to cylindrical or rod-like forms. This transformation is pivotal,

as cylindrical micelles provide a more confined environment conducive to the controlled growth of nanocrystals. Such confinement facilitates uniformity in size and distribution of gold nanocrystals, which is essential for various applications. The role of HT extends beyond micelle shape alteration; it also effectively reduces the energy barrier for nucleate release and adsorption to 2.83 ± 0.12 kcal/mol as compared to previous cases. This reduction is instrumental in overcoming some of the challenges associated with the strong interactions between the micelle layers, hydration shells, and the substrate. By weakening these interactions, HT enables a more efficient release of gold nucleates from the micelle to the gold surface, enhancing the nucleation and growth process.

Chapter 6
Role of Thiolated layer
in Reduction of Energy Barrier

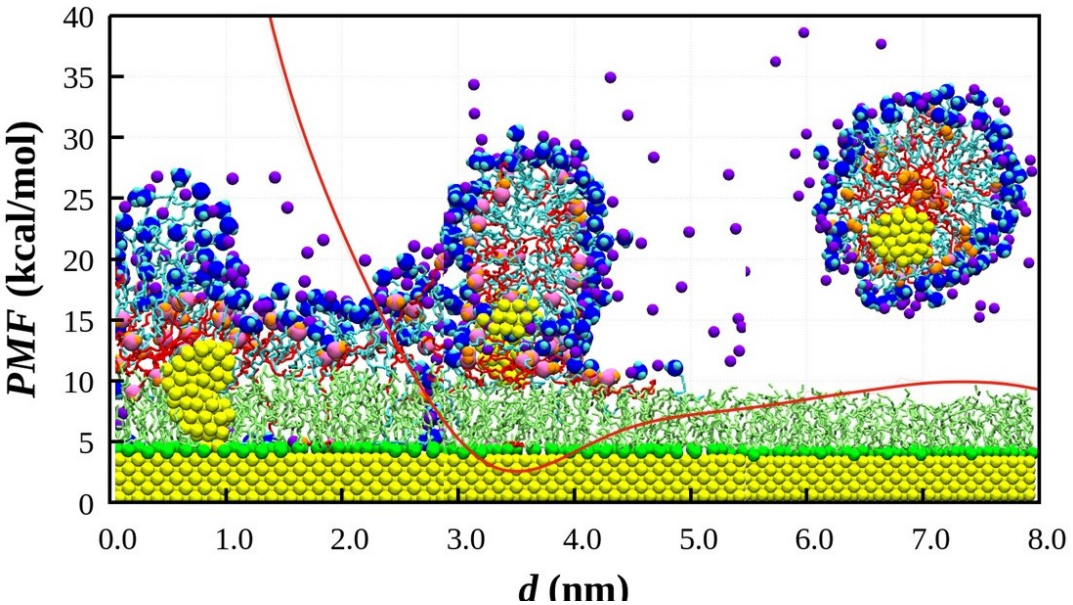

6.1 Introduction

Self-assembled monolayer (SAM) on solid substrates, formed by the adsorption of long-chain molecules through their head groups, represent a significant area of research due to their ability to create tunable surfaces with precisely defined size, shape, and composition. These molecular assemblies provide a versatile platform for fabricating functional surfaces with applications across various fields, including chemistry[215, 216], optics[217, 218], electronics[219], medicine[220], microfabrication[221, 222], and biology[223]. The properties of SAM, particularly those formed from alkanethiols, can be selectively modified by altering the functional groups at the head or tail while maintaining the overall chain conformation. This flexibility makes alkanethiol SAM highly adaptable for specific functional requirements. SAM can form on various solid substrates, such as

gold, silver, and silicon, through the spontaneous adsorption of molecules from a solution.[224] The exact arrangement and configuration of these molecules on the substrate surface have been debated for decades.

Self-assembly of surfactants depends strongly on the layering of water on a hydrophilic surface,[33, 225, 226] and they create aggregated structures. On the contrary, surfactants create a self-assembled monolayer under strong cohesive interactions between the hydrophobic tail group and the surface at lower coverage; whereas, at higher surface coverage, some of the surfactants leave the surface to create micelles at the bulk.[227] On a graphite surface, atomic force microscopy (AFM) image analysis indicates that sodium dodecyl sulfate (SDS) and cetyltrimethylammonium bromide (CTAB) tends to create a plane, hemispherical and hemicylindrical aggregates, parallel stripes based on the ionic strength and hemimicelles on a rough gold surface [228, 229]. The time required for equilibrium structure formation near the surface was also calculated [229].

Domínguez et al. studied self-aggregation of SDS on a graphite surface. At low surface coverage, SDS formed hemicylindrical aggregates, whereas, at high coverage, complete cylindrical structures emerged due to the formation of a water layer that created a hydrophilic environment. The SDS tails in cylinder-shaped structures were found to be straighter compared to those in hemicylinders.[34] Recently, Chowdhury et al.[156] have investigated the behaviour of sodium dodecyl sulfate (SDS) molecules at the mica/water interface and revealed the influence of temperature on the growth of self-assembled monolayers (SAM) of amphiphilic molecules, specifically n-octanol, and their impact on wetting behaviour and mass transfer dynamics on a mica surface.[230]

Recent studies have shed light on the structural arrangement of SAM, showing that sulfur atoms in alkanethiols bind to gold atoms on the substrate while the alkyl chains are closely packed and tilted at an angle of approximately 30° relative to the surface normal. Furthermore, exposing a gold surface to a solution containing a mixture of alkanethiols enables the formation of mixed SAM, where monolayers consist of a combination of gold-thiolate complexes.[59] This allows for the surface density of functional groups to be varied, offer-

ing additional opportunities for tailoring surface properties to specific applications. Ahn et al. demonstrated how SAM of alkyl thiols on gold surfaces evolves—from initial physisorption to densely packed layers.[37] Bhandary et al. have investigated the molecular dynamics of alkyl thiol adsorption on gold nanoparticles to form Janus nanoparticles with asymmetric surface coatings. The process involved a two-step mechanism, with thiol droplets initially binding to the gold surface ($\sim$ 1 ns) followed by diffusion-driven monolayer growth ($\sim$ 100 ns).[91]

In our previous study, the gold nucleates were stabilized within the micelle by favourable hydrophobic, electrostatic, and entropic interactions. However, the adsorption process faces resistance due to hydration layers and the need for micelle reorganization. The co-surfactant OLA was instrumental in reducing these challenges, enabling effective nucleate release and adsorption. Despite these improvements, a significant energy barrier persists, largely due to hydration layers and micelle reorganization requirements. Reducing this energy barrier is crucial for optimizing nucleation and growth processes. Therefore, we introduced sparingly dispersed thiol molecules on the gold surfaces and wanted to optimize the process via free energy estimation.

6.2 Models and Methodology

The simulation focused on modelling the formation of a sparingly dispersed thiol monolayer on a gold (111) surface using 1-hexadecane thiol (HT) molecules. Hexadecanethiol was modelled as a 16-carbon alkyl chain with a thiol headgroup, where CH_2 and CH_3

Table 6.1: Lennard-Jones (LJ) and Morse Potential Parameters of United Atoms

Nonbonded Interactions			
Atom	σ_{ij} **(Å)**	ϵ_{ij} **(kcal/mol)**	q **(e)**
CH_3	3.75	0.0914	0.0
CH_2	3.75	0.1947	0.0
CH_2(S)	3.75	0.1947	0.171
SH	3.62	0.461	-0.171
Morse	D_e **(kcal/mol)**	r_0 **(Å)**	α **(Å^{-1})**
Au-S	8.763	2.65	1.47

groups were treated as united atoms. The gold (111) surface consisted of three atomic layers in an FCC lattice and a lattice constant of 4.065 Å.

Initially, 108 HT molecules were randomly distributed on the gold surface. The simulations were conducted using a combination of force field parameters, including harmonic potentials for bond stretching and angle bending, and a triple cosine function to model torsion interactions, capturing the conformational flexibility of the alkyl chains. GROMOS96 53a6 forcefield[93] was used to model the bonded and non-bonded interactions for CTAB, OLA and HT molecules. An extended Simple Point Charge (SPC/E) water model was used to model the solvent. Non-bonded interactions were modelled using the Lennard-Jones (LJ) potential, while the sulfur-gold (S-Au) interaction was represented using a hybrid potential. This hybrid potential was employed by incorporating a Morse potential for distances below 4.4 Å, and an LJ potential for distances beyond 4.4 Å.[37] The LJ and Morse parameters for each atom are listed in Table 6.1. Lorentz-Berthelot (LB) combination rules were applied to calculate cross-interactions between heteroatomic pairs, ensuring consistent force field parameters.[214] The simulation used LJ parameters for gold atoms as reported by Heinz et al.[231] Periodic boundary conditions were employed in all three spatial directions to replicate an infinite system and minimize edge effects. Molecular dynamics simulations were carried out using LAMMPS[211], and VMD[150] was used to visualize the simulation trajectories.

To ensure system stability, the initial configuration underwent an energy minimization procedure using the steepest descent method for 5000 steps. This step reduced any unfavorable interactions and prepared the system for subsequent molecular dynamics simulations. After a 10 ns equilibration run, the HT molecules self-assembled into a monolayer on the gold surface, as shown in Figure 6.1(a). The sulfur atoms in the SH groups adsorbed strongly onto the gold surface, while the alkyl tails (CH_2 and CH_3 groups) oriented away from the surface, creating a hydrophobic layer on gold (111) surface.

The energy landscape for the fusion of nucleates with the gold surface was calculated using the umbrella sampling technique[155] followed by the Weighted Histogram Analysis

Method (WHAM) [154]. In the umbrella sampling, a series of 70 linearly spaced windows along the reaction coordinate, defined by the distance between the centre of mass of the nucleate and the apex of the gold surface, were subjected to an external biasing potential to facilitate comprehensive sampling within these windows. A harmonic potential, $u_i = \frac{1}{2}k(r - r_i)^2$ used as the external biasing potential at window i, where r_i represents the reference location and k denotes the harmonic force constant. We utilized the Weighted Histogram Analysis Method (WHAM) to remove the biasing potential and reconstruct the potential of mean force (PMF).[154] The reaction coordinate defined as the distance between the centre of mass of gold nucleate and the upper surface of the gold (111) surface was the reaction coordinate. A 1.0 ns production runs were conducted in an NVT ensemble for each window at 303.15 K, employing restraints with a harmonic force constant of 100 kcal/mol.Å^2. In WHAM, the calculation of PMF involved setting the number of bins to 100, accompanied by a tolerance for iterations of 10^{-5}. We monitored the size and shape of the micelle by calculating the components of the radius of gyration (R_g) tensor, $R_{g_{xx}}$, $R_{g_{yy}}$, $R_{g_{zz}}$, respectively. The radius of gyration R_g of the micelle was calculated using the equation: $R_g = \sqrt{(\sum_{i=1}^{N}(R_i - R_{COM})^2)/N}$ where, N is the total number of atoms in the micelle, R_{COM} is the center of mass (COM) of that micelle, and R_i is the position of the i^{th} atom in the micelle. We calculated the order parameter to understand the orientation of the molecules within the micelle on the gold surface. The order parameter of the micelle molecules is a measure of the degree of ordering and alignment of CTAB molecules within a micelle structure. The order parameter expressed as $S_{zz} = (3cos^2\theta_i - 1)/2$ where, θ_i is the angle between the end-to-end vector of the i^{th} molecule and the surface normal vector.

6.3 Result and Discussion

We have started our discussion with the density profile of water, micelle and thiol molecules along the z-dimension to understand the formation of the hydration layer by water molecules on the thiol layer, the distributions of thiol molecules on the surface.

Figure 6.1(a) depicts the functionalization of a gold (111) surface with hexadecanethiol

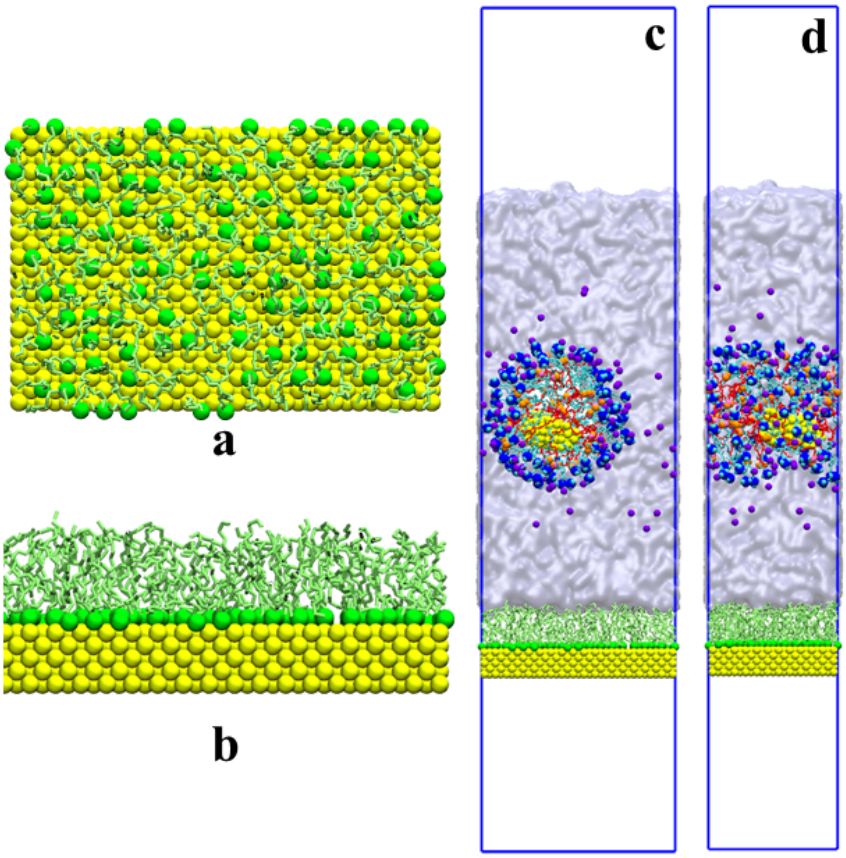

Figure 6.1: a, b – Dispersed hexadecane thiol monolayer on a gold (111) surface – top and side view, respectively. The thiol groups are represented as green spheres, respectively, and all the methyl groups are represented in green. c,d – Cross-sectional (xz-plane) and longitudinal (along y-axis) view, respectively, of the cylindrical micelle formed by CTAB and OLA. For CTAB molecules, the nitrogen atoms and bromide ions are represented as blue and purple spheres, respectively, and all the methyl groups are represented as cyan-colored bonds. For OLA molecules, the nitrogen atoms and hydrogen atoms are represented as pink and orange spheres, respectively, and all the methyl groups are represented as red-colored bonds. Water has shown an ice-blue colour in continuous media. The blue rectangle represents the periodic simulation box.

molecules. The thiol groups, responsible for bonding with the gold surface, are represented as green spheres, while the methyl groups of the alkyl chain are depicted in green, highlighting the formation of a hydrophobic monolayer on the surface. This functionalisation creates a structured interface that can influence the interactions with nearby molecules, such as surfactants and micelles. Figure 6.1(b) The front view of the hexadecane thiol monolayer shows the structural orientation of the thiol molecules on the gold (111) surface. The thiol molecules are aligned vertically, with their sulfur atoms bound to the gold surface and their methyl groups extending outward, creating a hydrophobic in-

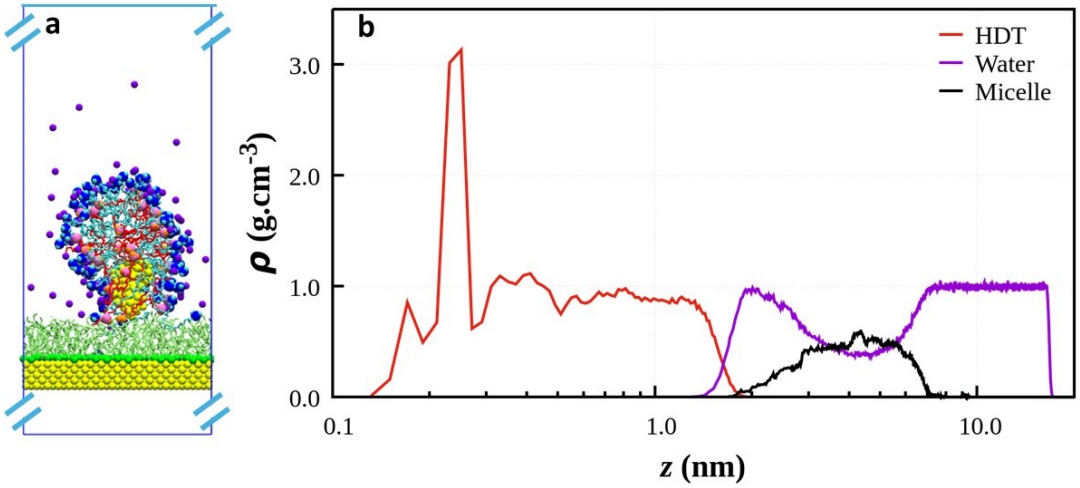

Figure 6.2: (a) Snapshot of the system containing a cylindrical micelle of co-surfactant OLA with CTAB molecules on the thiol-functionalized gold surface in an aqueous media. The Au(111) surface, at the bottom, is represented in yellow spheres. Water has shown an ice-blue color continuous media. The blue rectangle represents the periodic box (not to scale in the z-direction). (b) Density profile of water, micelle and thiol molecules along the z-axis

terface. This arrangement ensures the stability of the monolayer and provides a structured surface for interactions with the micelle. Figure 6.1(c) represents a cross-sectional view (xz-plane) of the cylindrical micelle formed by CTAB and OLA molecules after a production run. In this micelle, the nitrogen atoms of CTAB and bromide ions are shown as blue and purple spheres, respectively, while the methyl groups of CTAB are in cyan. Nitrogen and hydrogen atoms are depicted as pink and orange spheres for the OLA molecules, respectively, with the methyl groups in red. This visualisation revealed the spatial organisation of the micelle, where CTAB molecules form the outer shell, and OLA molecules occupy the core. Bromide ions stabilise the structure near the positively charged nitrogen headgroups of CTAB. Figure 6.1(d) shows the micelle system along the y-axis, providing a snapshot of the micelle interacting with the surrounding medium. The water molecules are depicted as a continuous ice-blue medium, showing how the micelle is suspended in an aqueous environment. The blue rectangle outlines the periodic simulation box used for molecular dynamics, replicating a bulk solution to ensure realistic modelling. This visualization highlights the micelle's structural stability and the dynamic interaction between its components and the surrounding solvent during the simulation.

Figure 6.2 (a) shows a snapshot of the system containing a cylindrical micelle of OLA co-surfactant with CTAB molecules on the thiol-functionalized gold surface in an aqueous medium. Figure 6.2 (b) depicts the density profiles of water, micelles, and thiol molecules along the z-axis, providing insight into their spatial distribution in the simulation system. The sharp peak represented by the red line near the surface (at ~ 0.2 nm) indicated that HDT molecules are strongly adsorbed onto the Au(111) gold surface. The water density profile represented by the blue line indicates that the density increases sharply near the thiol layer, indicating a hydration layer forming due to interactions with HDT molecules. The broadening of the water density near the micelle suggests the formation of a hydration layer. Beyond this region, the water density stabilises at a constant value, representing the bulk phase of water. The micelle density profile exhibits a distinct peak represented by the black line at ~ 4.25 nm, corresponding to the location of the micelle layer. The overlap between the red and blue curves suggested interactions between the micelle and surrounding water molecules. This interaction contributes to the hydration layer and micelle stability.

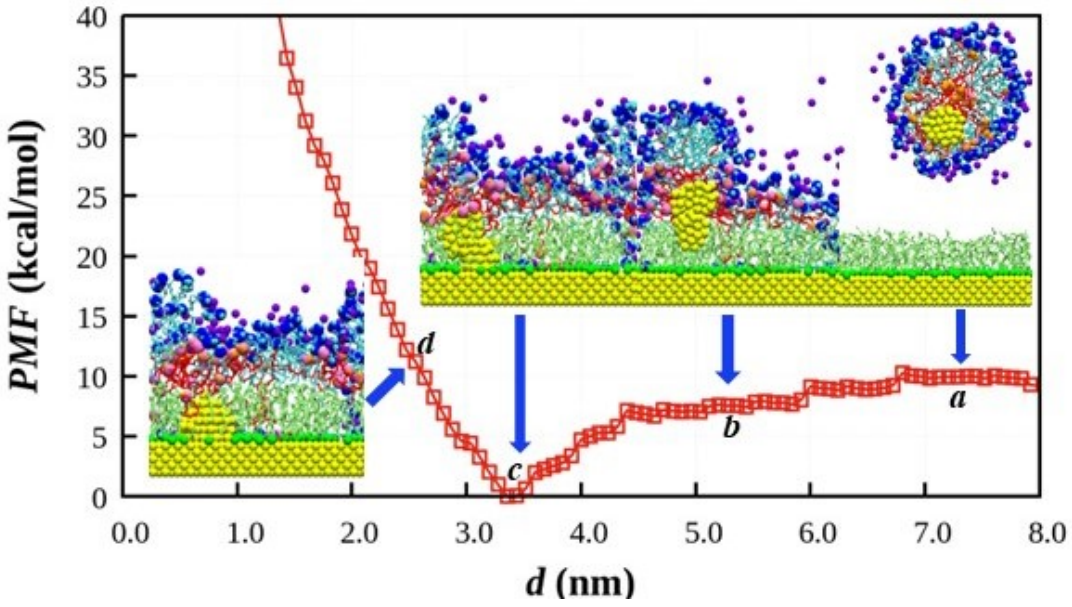

Figure 6.3: Potential of Mean Force (PMF) as a function of the distance (d) between the gold nucleate and the functionalized gold surface with hexadecane thiol molecules. Insets depict the structural configurations of the micelle containing gold nucleate at various stages along the reaction coordinate. The black arrows indicate the position of the nucleate from the apex of the thiolated layer on the gold surface. The color codes for molecular presentation are the same as in Figure 6.1, and water is omitted for visual clarity.

Figure 6.3 depicts the potential of mean force (PMF) profile for the interaction of a gold

nucleate encapsulated within a CTAB-OLA micelle with a hexadecanethiol-functionalised gold surface, providing critical insights into the energy landscape and structural evolution of the system during this process. At point "a" ($\sim$ 7.0 nm), the micelle resides in its most stable configuration in the bulk solvent. In this state, it retains its spherical integrity, and the encapsulated gold nucleate remains shielded by the surfactant molecules, with only weak long-range interactions (e.g., van der Waals forces) between the micelle and the surface. As the micelle moves closer to the thiolated layer on the gold surface, point "b" ($\sim$ 5.0–6.0 nm) marks the onset of steric and hydrophobic interactions imposed by the hexadecane thiol-functionalized surface. This leads to initial structural deformation of the micelle and an increase in PMF, reflecting the work required to overcome these interactions. At point "c" ($\sim$ 4.0 nm), the PMF reaches a local maximum, indicating the presence of a significant energy barrier. This energy barrier arises from the steric and hydrophobic effects of the dodecanethiol layer, which resist further approach of the micelle. Corresponding structural changes in the micelle include partial deformation, with the encapsulated gold nucleate remaining shielded but in closer proximity to the surface. Overcoming this energy barrier is a critical step that enables the micelle to transition to the near-surface interaction state. At point "d" ($\sim$ 2.5–3.0 nm), the PMF decreases sharply, signifying the formation of strong interactions between the micelle and the functionalized surface. At this stage, the micelle undergoes substantial deformation, flattening against the surface, and the surfactants rearrange to facilitate closer contact between the encapsulated gold nucleate and the gold surface. Strong van der Waals interactions dominate, stabilizing the system in a new energy minimum.

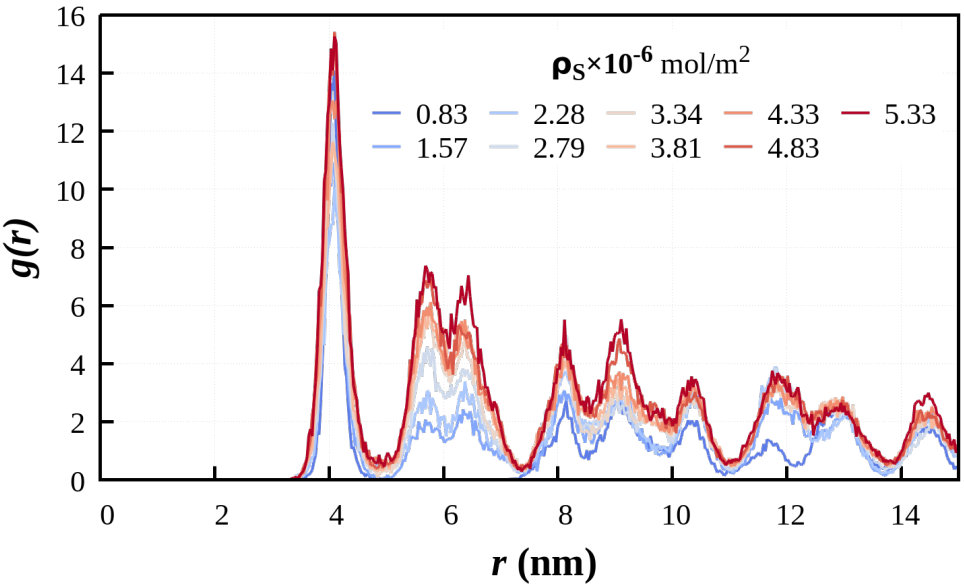

Figure 6.4: In-plane pair correlations (radial distribution function) between thiol molecules on Au(111) surface. Blue to red color gradient represents the RDF profiles at different surface densities of thiol molecules.

Figure 6.4 In-plane correlations (radial distribution functions) between thiol molecules adsorbed on an Au(111) surface. At low surface density of thiol molecules, the RDF shows fewer pronounced peaks, indicating a less ordered arrangement of molecules due to the larger spacing between them. As the surface density increases (blue to red), the peaks become more prominent and shift slightly, indicating tighter packing and enhanced ordering of the thiol molecules. At higher surface density of thiol molecules, the RDF shows sharper and more distinct peaks, suggesting increased molecular ordering as the molecules are packed more closely.

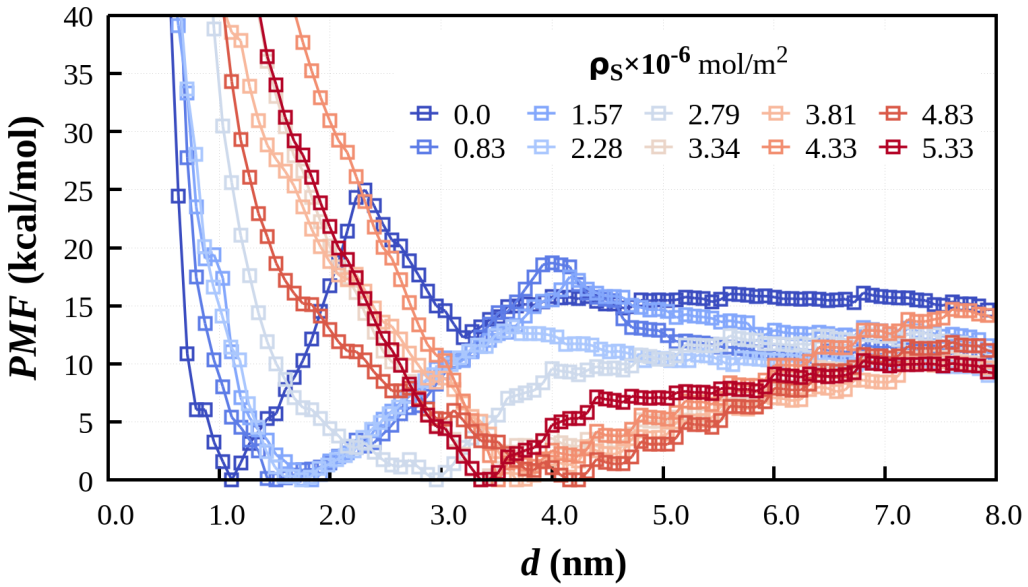

Figure 6.5: Potential of Mean Force (PMF) as a function of the distance (d) between the centre of mass of the gold nucleate and the thiol-functionalized gold surface for various surface densities of thiol molecules. Blue to red color gradient represents the PMF profiles at different surface densities of thiol molecules.

Figure 6.5 shows the effect of thiol surface density on the Potential of Mean Force (PMF) for the interaction between a gold nucleate encapsulated within a CTAB-OLA micelle and a thiol-functionalized gold surface. The PMF profiles, plotted as a function of the distance (d) between the centre of mass of the gold nucleate and the surface, show a clear trend: as the surface density of thiols (ρ_S) increases, the energy barrier decreases significantly. This reduction in the energy barrier is primarily attributed to the hydrophobic nature of the thiol layer, which facilitates stronger micelle-surface interactions and stabilizes the gold nucleates. At lower thiol densities, the PMF profiles exhibit steep energy barriers, indicating higher resistance to the micelle towards the thiolated layer. In contrast, higher thiol densities result in a downward shift of the PMF curves, reflecting reduced resistance and enhanced stabilization of the nucleate on the surface. The energy minimum observed at shorter distances ($\sim$ 2.0–3.0 nm) becomes more pronounced with increasing thiol density, representing the most stable configuration of the micelle and nucleate on the surface. This enhanced stabilization is due to stronger hydrophobic and steric interactions provided by the densely packed thiol layer.

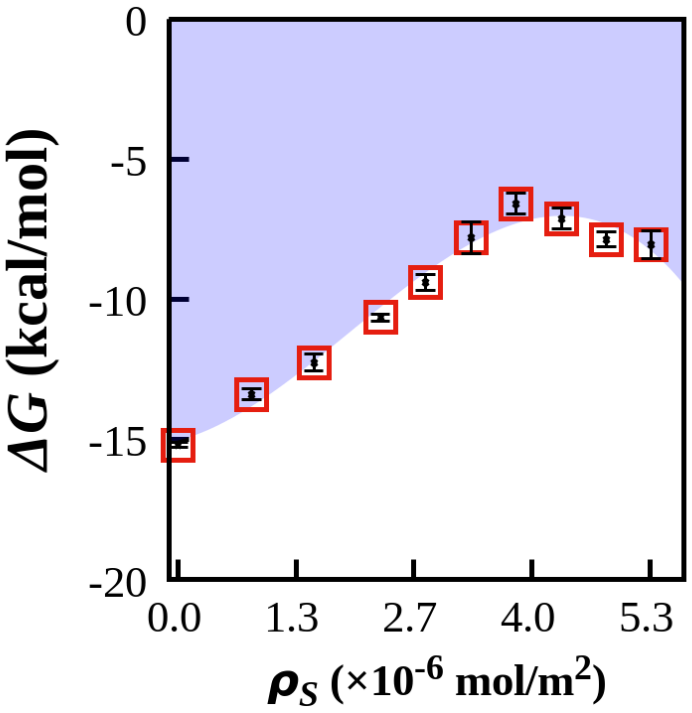

Figure 6.6: Change in free energy (ΔG) as a function of the surface density of thiol molecules (ρ_S)

Figure 6.6 illustrates the relationship between the change in free energy (ΔG) and the surface density of thiol molecules (ρ_S). The ΔG values remain negative throughout, indicating that the process is thermodynamically favorable at all thiol densities. However, as the surface density increases, there is a gradual decrease in the magnitude of ΔG, with the system reaching a plateau at higher thiol densities. The negative free energy values suggest that the introduction of a thiol layer significantly enhances the thermodynamic stability of thiol. This stabilization is primarily attributed to the hydrophobic interactions between the thiol molecules and the micelle, as well as the structural rearrangements within the micelle that optimize its interaction with the functionalized surface. As the thiol density increases, the more favorable interactions reduce the energy barrier for adsorption and nucleation, further facilitating the growth of gold nucleates on the surface. The plateau observed at higher thiol densities indicates a saturation effect, where further increases in thiol density provide diminishing returns in terms of free energy changes. The Optimum surface density is 3.34×10^{-6} mol/m^2.

6.4 Summary

This PMF profile highlights the critical role of surface functionalization in tuning the interaction dynamics between nanoparticles and surfaces. The introduction of the hexadecanethiol layer significantly increases the energy barrier compared to an unfunctionalized surface, demonstrating the importance of steric and hydrophobic effects in modulating interaction forces. These findings provide valuable insights into the molecular-level mechanisms governing nanoparticle-surface interactions and offer guidelines for designing functionalized surfaces to optimize nanomaterial synthesis and surface engineering. The thiol layer reduces the energy barrier; the Optimum surface density is 3.34×10^{-6} mol/m^2. This behavior highlights the importance of optimizing the thiol surface density to balance stability and efficiency during nanoparticle synthesis. Overall, the results underscore the critical role of surface functionalization in promoting thermodynamic favorability and facilitating micelle-mediated nucleation processes.